Supplementary Information

Trace-LiCl-assisted Synthesis of High-Loading Ordered Pt_3Co Intermetallic Catalysts for Oxygen Reduction Reaction in Fuel Cells

Yutao Ni[a,b], Jiahui Song[a,b], Huiying Lan[a], Xue Jing,[a,b] Wenwen Shi[a,*], Ruimin Ding[a,*], Xi Yin[a,*]

[a] State Key Laboratory of Coal Conversion, Institute of Coal Chemistry, Chinese Academy of Sciences, Taiyuan, Shanxi 030001, China

[b] School of Chemical Engineering, University of Chinese Academy of Sciences, Beijing 100049, China

[*]Corresponding author. E-mail addresses: shiwenwen@sxicc.ac.cn (W. Shi), dingrm@sxicc.ac.cn (R. Ding), xiyin@sxicc.ac.cn (X. Yin).

Number of pages: 32

Number of figures: 21

Number of tables: 8

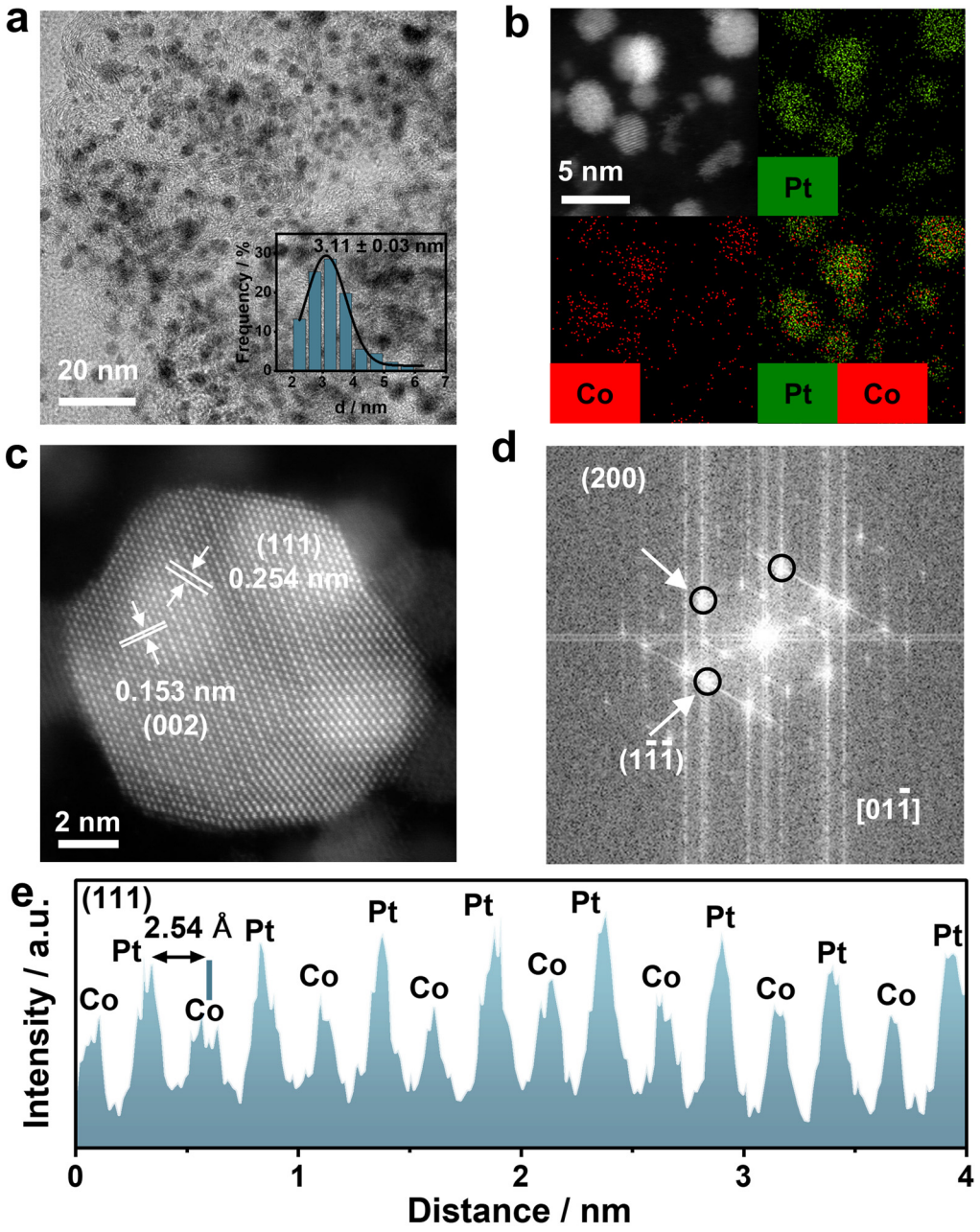

Figure S1. (**a**) Representative TEM image of $Pt_3Co/C(Li_{0.0})$-700 °C-2 h. (**b**) EDS-mapping images of $Pt_3Co/C(Li_{0.0})$-700 °C-2 h. (**c**) Atomic-resolution HAADF-STEM image of $Pt_3Co/C(Li_{0.0})$-700 °C-2 h. (**d**) FFT patterns of highlighted area from (c). (**e**) Line profile of $Pt_3Co/C(Li_{0.0})$-700 °C-2 h from part (c).

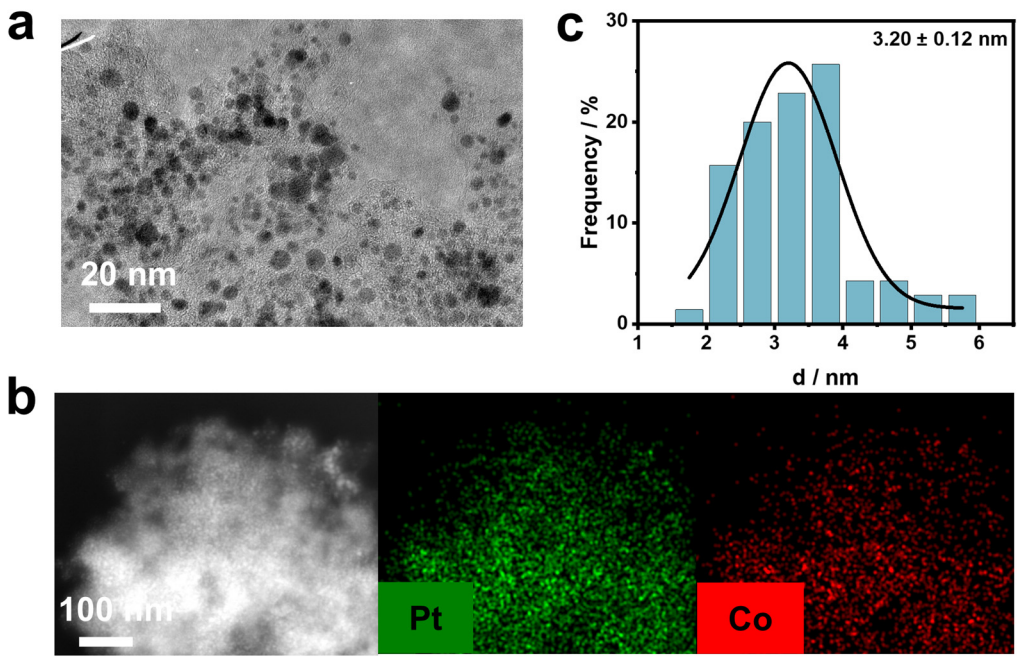

Figure S2. (**a**) Representative TEM image of $Pt_3Co/C(Li_{0.3})$-700 °C-2 h. (**b**) EDS-mapping of $Pt_3Co/C(Li_{0.3})$-700 °C-2 h. (**c**) Corresponding particle size distribution histogram derived from (a), with mean diameter indicated.

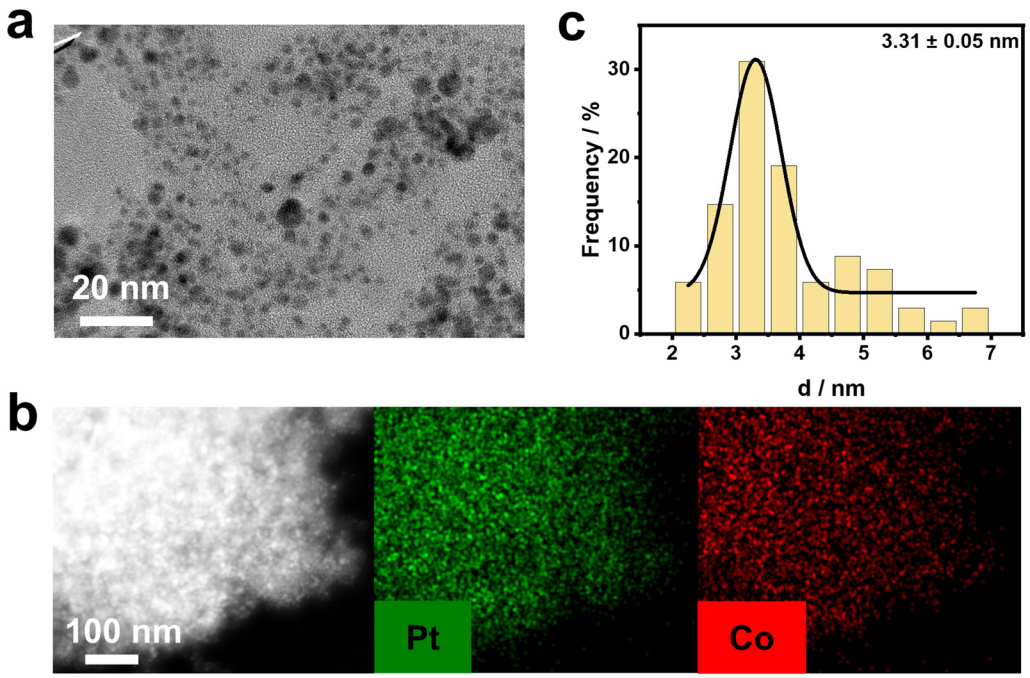

Figure S3. (**a**) Representative TEM image of $Pt_3Co/C(Li_{0.5})$-700 °C-2 h. (**b**) EDS-mapping of $Pt_3Co/C(Li_{0.5})$-700 °C-2 h. (**c**) Corresponding particle size distribution histogram derived from (a), with mean diameter indicated.

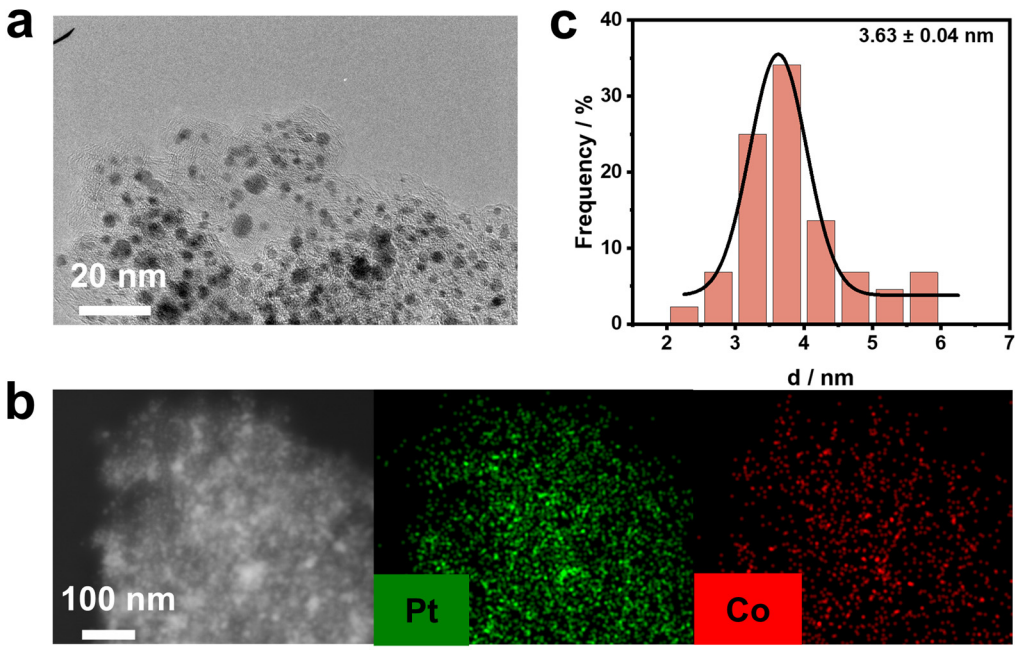

Figure S4. (**a**) Representative TEM image of $Pt_3Co/C(Li_{0.7})$-700 °C-2 h. (**b**) EDS-mapping of $Pt_3Co/C(Li_{0.7})$-700 °C-2 h. (**c**) Corresponding particle size distribution histogram derived from (a), with mean diameter indicated.

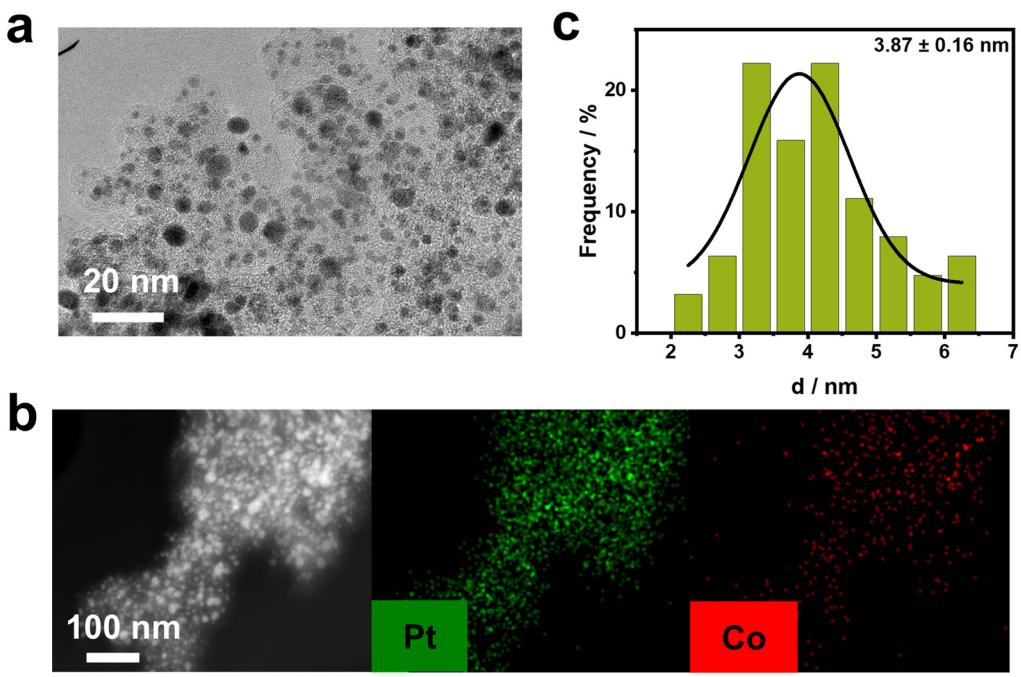

Figure S5. (**a**) Representative TEM image of $Pt_3Co/C(Li_{1.0})$-700 °C-2 h. (**b**) EDS-mapping of $Pt_3Co/C(Li_{1.0})$-700 °C-2 h. (**c**) Corresponding particle size distribution histogram derived from (a), with mean diameter indicated.

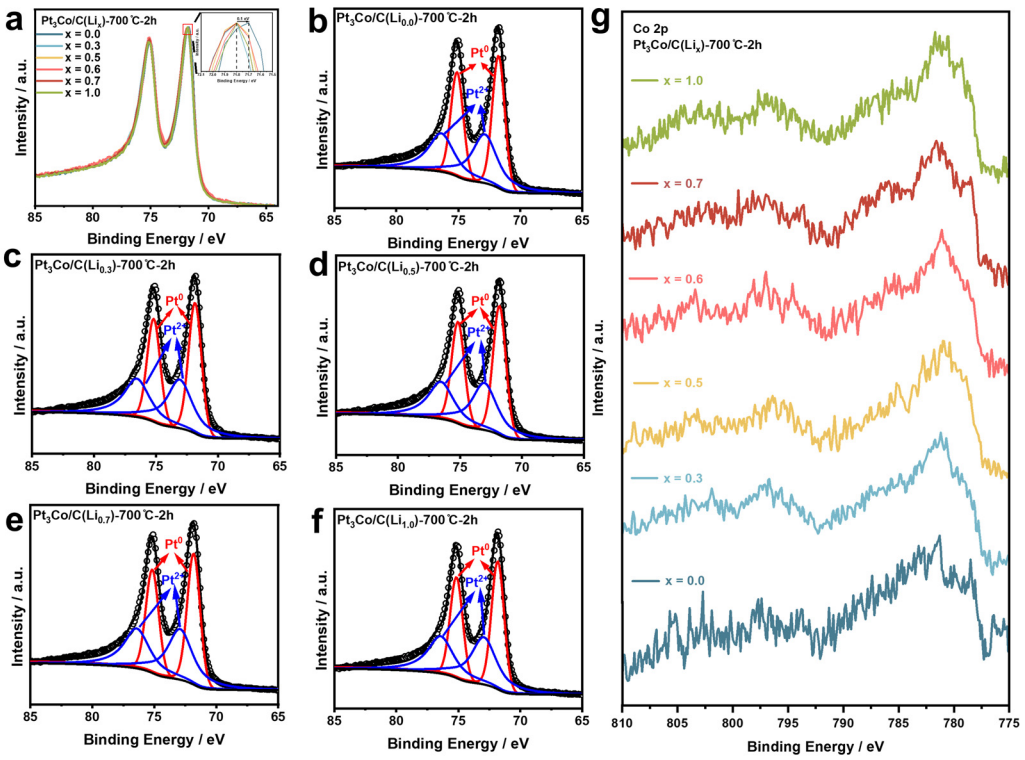

Figure S6. (**a**) High-resolution Pt 4*f* XPS of $Pt_3Co/C(Li_x)$-700 °C-2 h. High-resolution Pt 4*f* XPS and the corresponding peak deconvolution of (**b**) $Pt_3Co/C(Li_{0.0})$-700 °C-2 h (**c**) $Pt_3Co/C(Li_{0.3})$-700 °C-2 h (**d**) $Pt_3Co/C(Li_{0.5})$-700 °C-2 h (**e**) $Pt_3Co/C(Li_{0.7})$-700 °C-2 h (**f**) $Pt_3Co/C(Li_{1.0})$-700 °C-2 h. (**g**) High-resolution Co 2*p* XPS of $Pt_3Co/C(Li_x)$-700 °C-2 h (Weak signal not fitted for analysis).

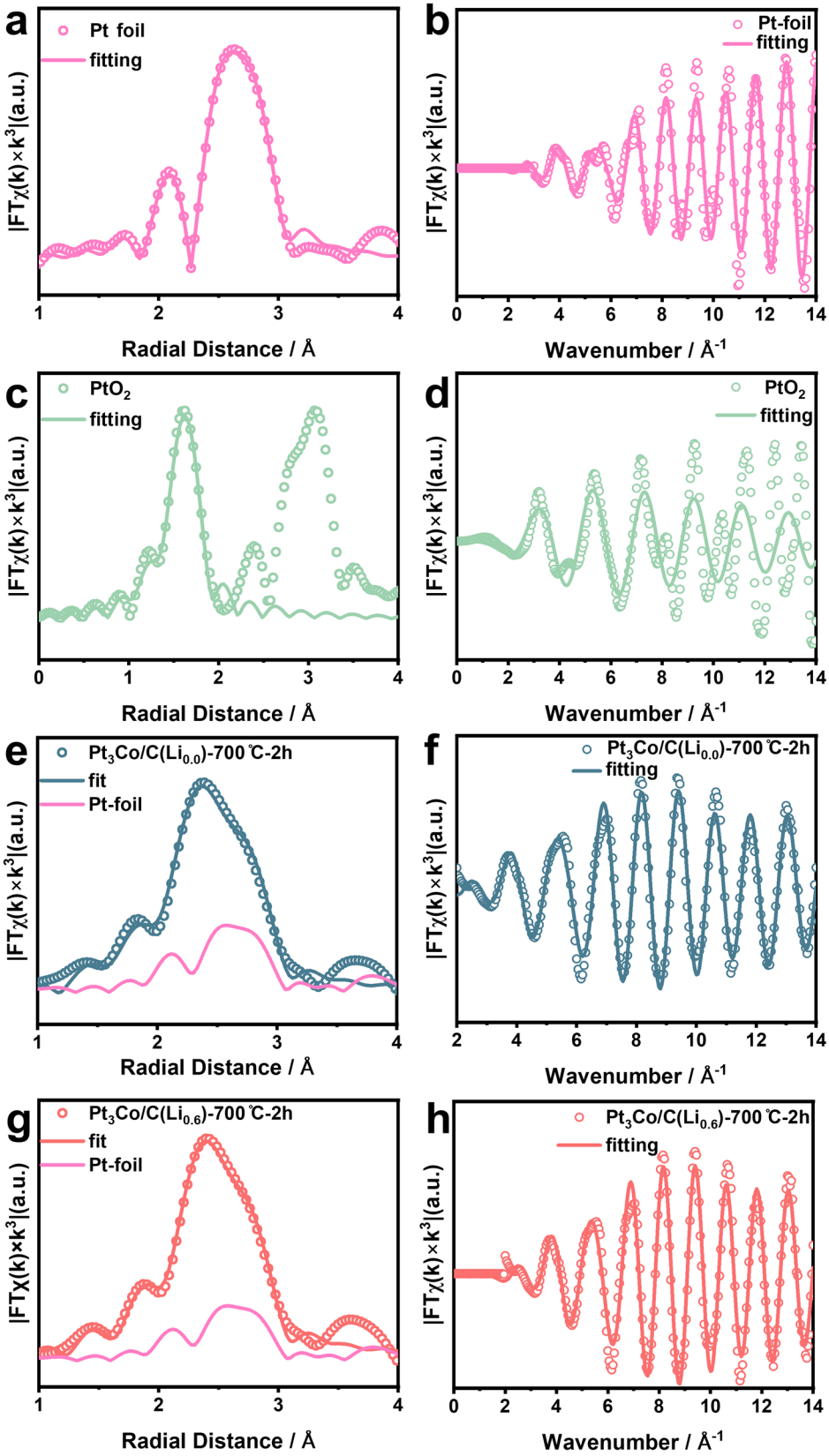

Figure S7. FT-EXAFS curves and EXAFS oscillation function and corresponding fitting curve at Pt L_3-edge of Pt foil ((**a**) and (**b**)), PtO_2 ((**c**) and (**d**)), $Pt_3Co/C(Li_{0.0})$-

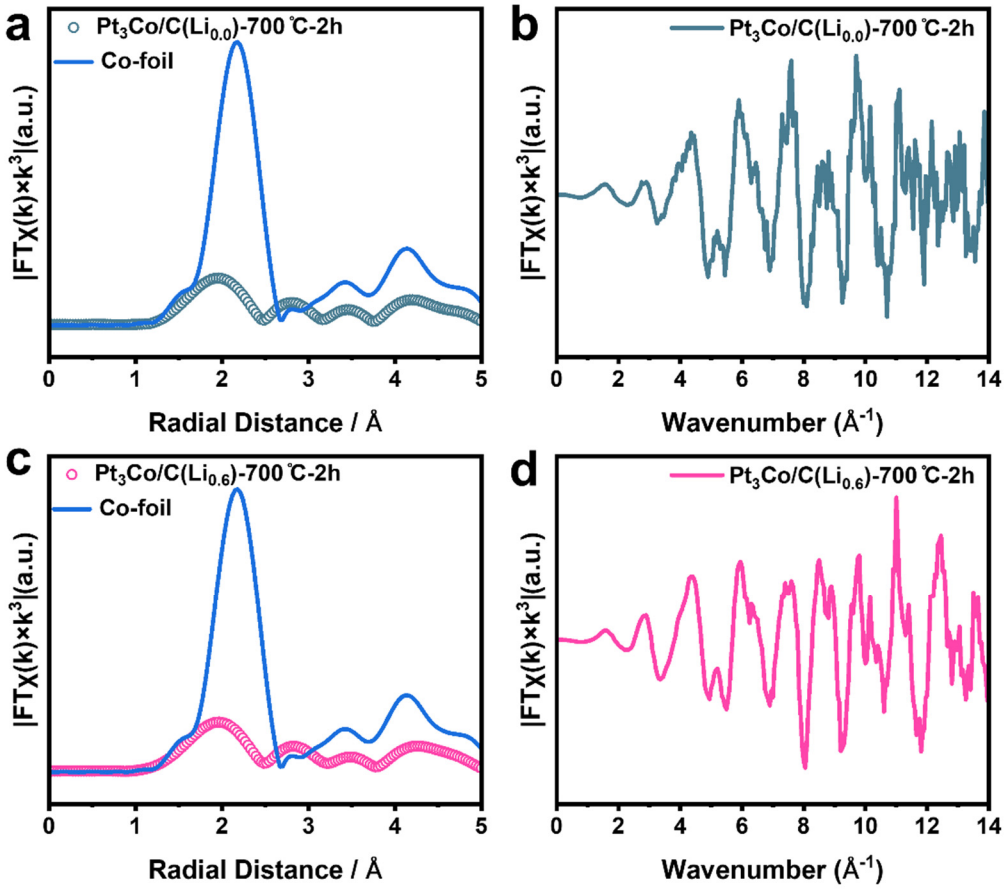

700 °C-2 h ((**e**) and (**f**)), $Pt_3Co/C(Li_{0.6})$-700 °C-2 h ((**g**) and (**h**)).

Figure S8. FT-EXAFS curves and EXAFS oscillation function at Co K-edge of $Pt_3Co/C(Li_{0.0})$-700 °C-2 h ((**a**) and (**b**)), $Pt_3Co/C(Li_{0.6})$-700 °C-2 h ((**c**) and (**d**)) (Weak signal not fitted for analysis).

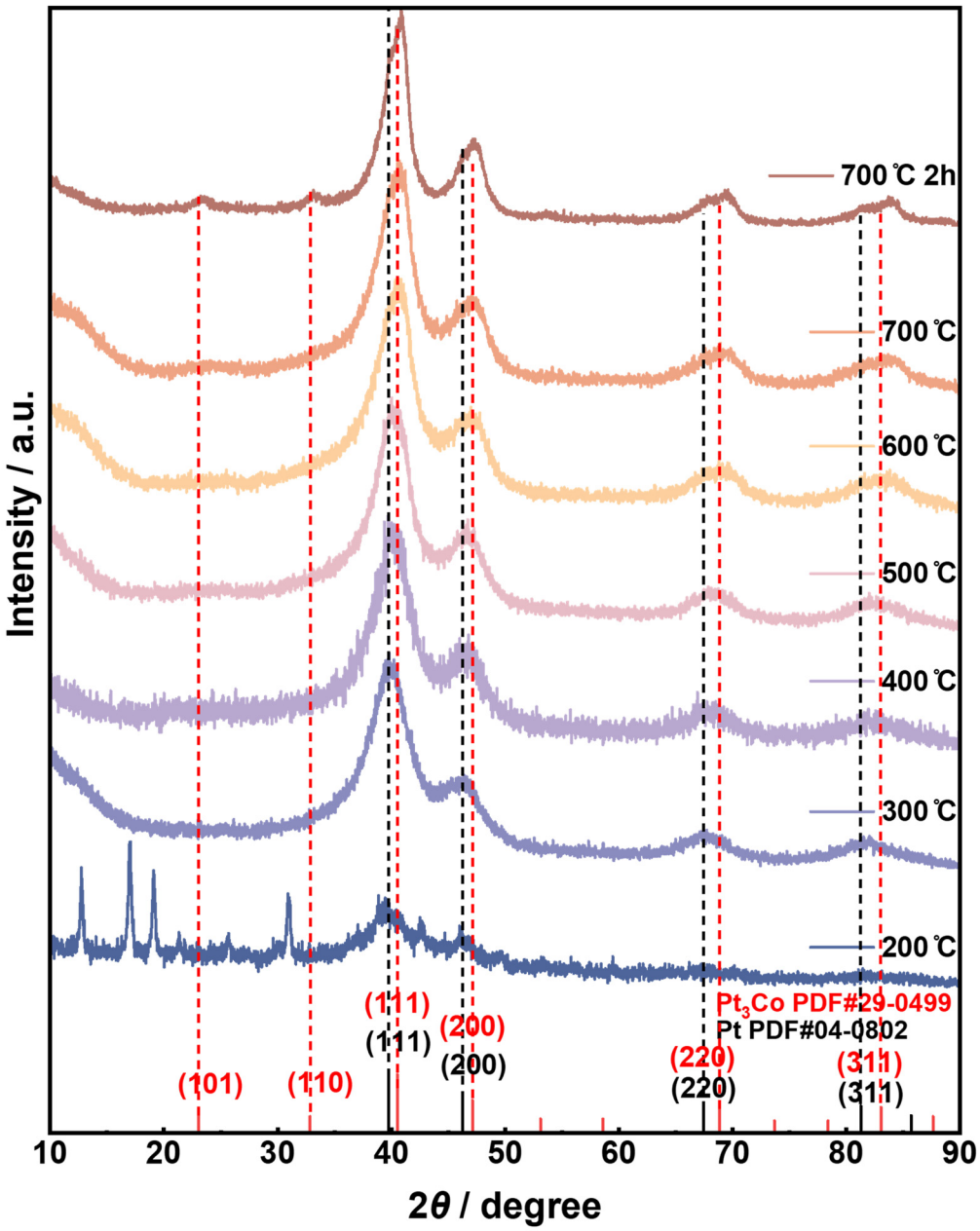

Figure S9. Temperature/time-evolution ex-situ XRD patterns of $Pt_3Co/C(Li_{0.0})$-700 °C-2 h catalyst during the annealing process.

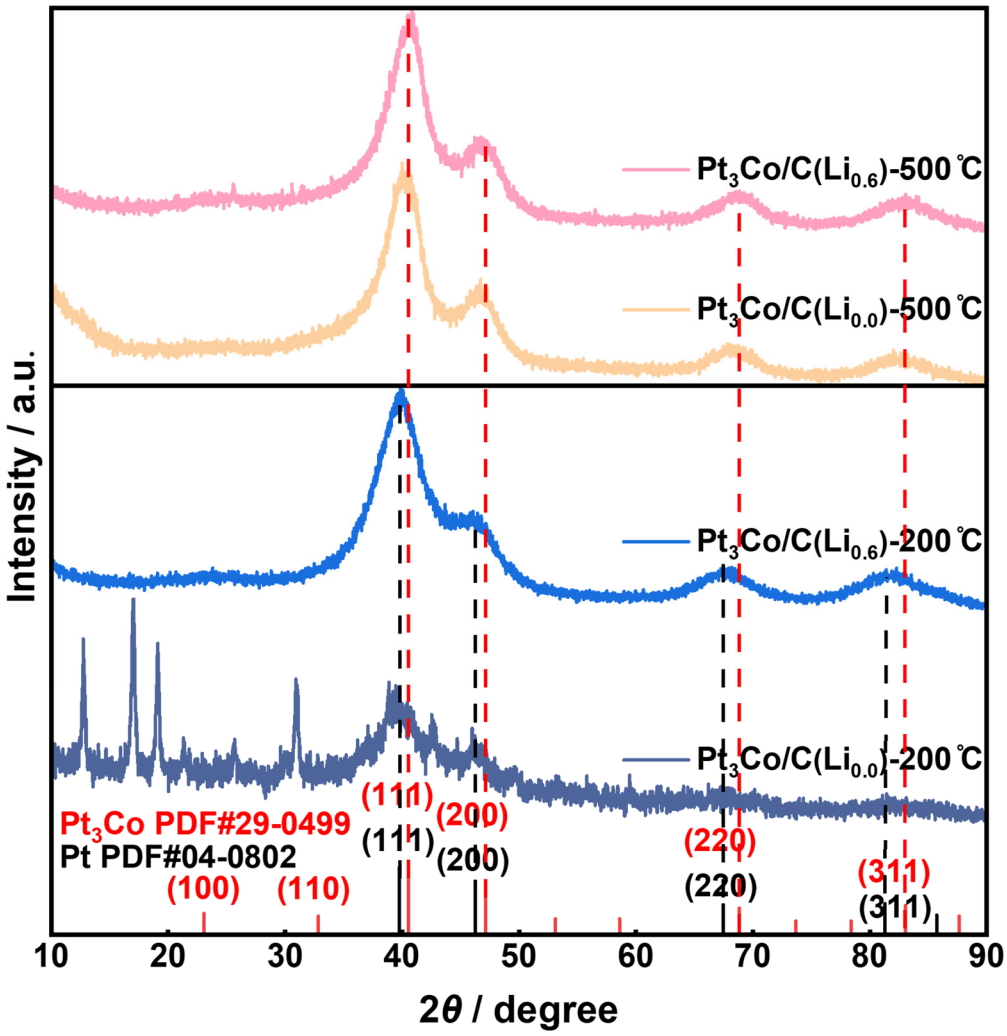

Figure S10. XRD patterns of $Pt_3Co/C(Li_{0.0})$-200°C, $Pt_3Co/C(Li_{0.6})$-200°C, $Pt_3Co/C(Li_{0.0})$-500°C and $Pt_3Co/C(Li_{0.6})$-500°C.

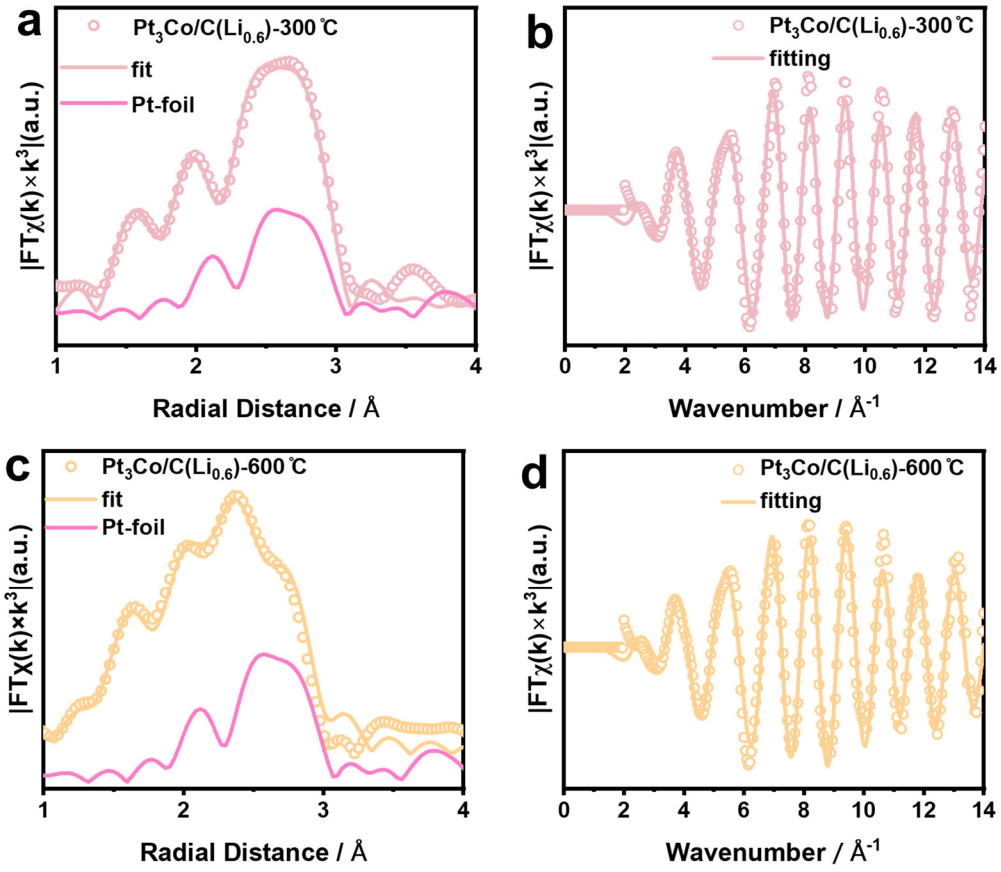

Figure S11. (**a**) FT-EXAFS curves at Pt L_3-edge of $Pt_3Co/C(Li_{0.6})$-300°C. (**b**) EXAFS oscillation function at Pt L_3-edge of $Pt_3Co/C(Li_{0.6})$-300°C. (**c**) FT-EXAFS curves at Pt L_3-edge of $Pt_3Co/C(Li_{0.0})$-600°C. (**d**) EXAFS oscillation function at Pt L_3-edge of $Pt_3Co/C(Li_{0.0})$-600°C.

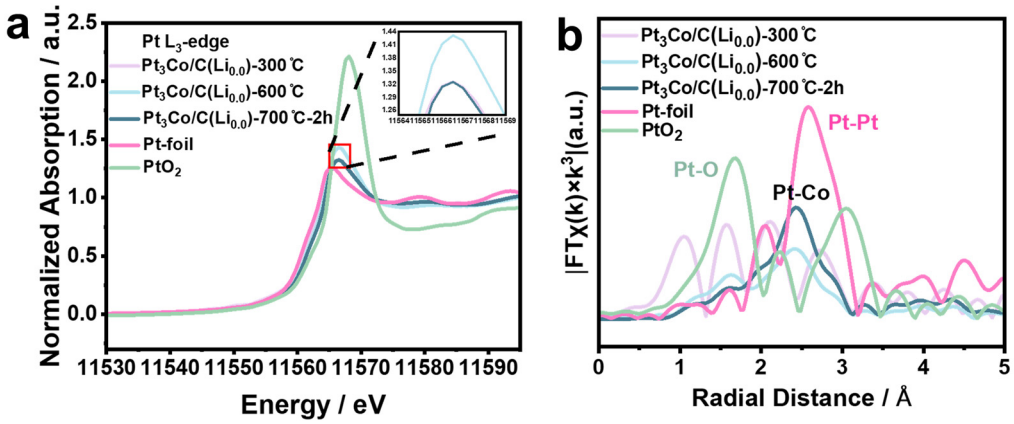

Figure S12. (**a**) Pt L_3-edge normalized XANES spectra of Pt foil, PtO_2, $Pt_3Co/C(Li_{0.0})$-300°C, $Pt_3Co/C(Li_{0.6})$-600°C and $Pt_3Co/C(Li_{0.6})$-700 ° C-2 h. (**b**) Corresponding FT-EXAFS spectra of (a).

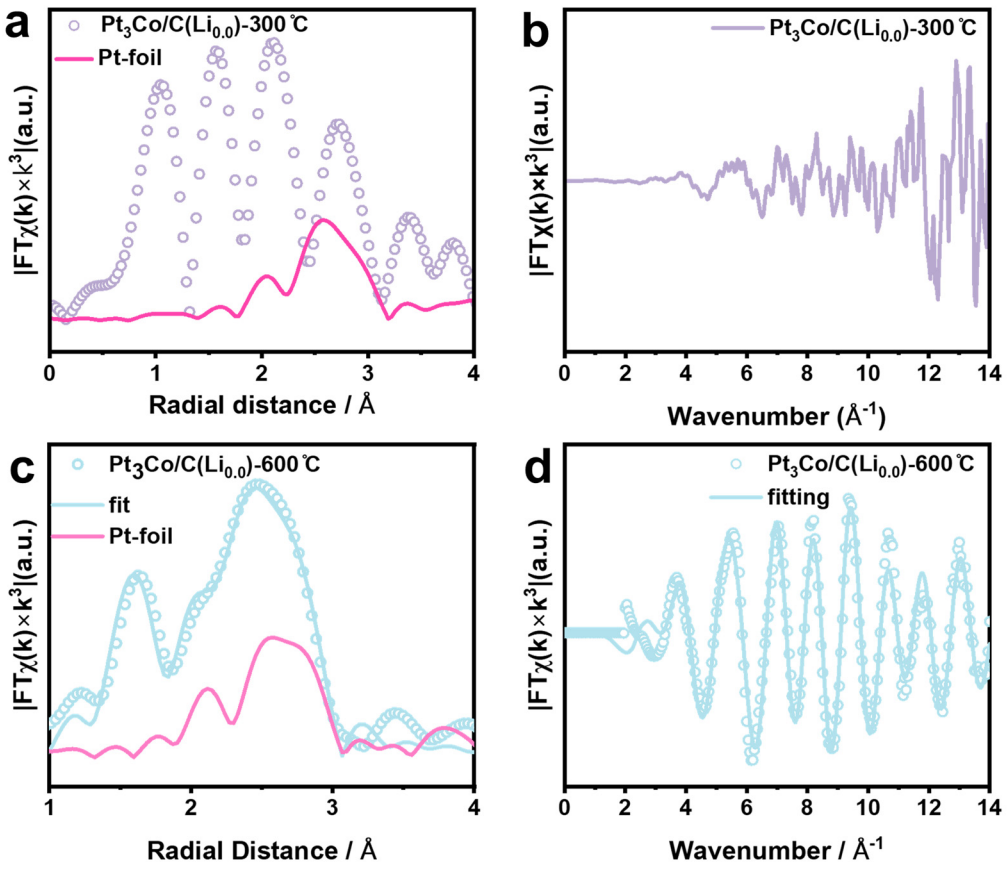

Figure S13. (**a**) FT-EXAFS curves at Pt L_3-edge of $Pt_3Co/C(Li_{0.0})$-300°C. (**b**) EXAFS oscillation function at Pt L_3-edge of $Pt_3Co/C(Li_{0.0})$-300°C (Weak signal not fitted for analysis). (**c**) FT-EXAFS curves at Pt L_3-edge of $Pt_3Co/C(Li_{0.0})$-600°C. (**d**) EXAFS oscillation function at Pt L_3-edge of $Pt_3Co/C(Li_{0.0})$-600°C.

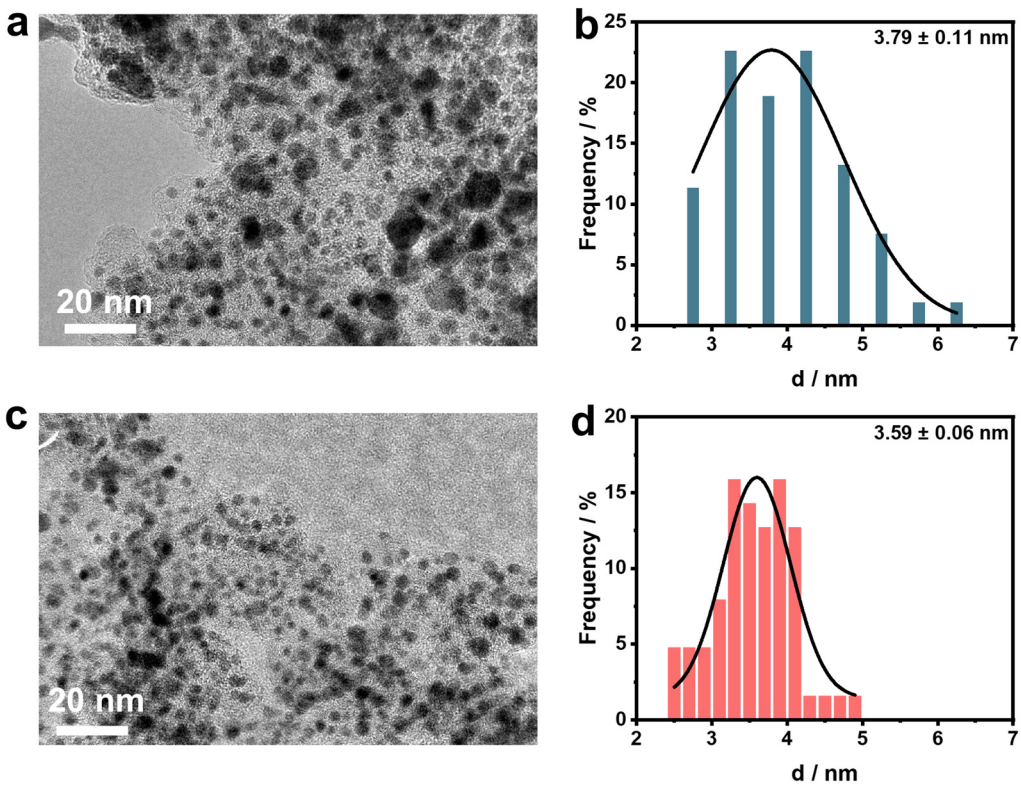

Figure S14. (**a**)TEM images of $Pt_3Co/C(Li_{0.0})$-700 °C-2 h after ADT. (**b**) Size distribution histogram of $Pt_3Co/C(Li_{0.0})$-700 °C-2 h after ADT. (**c**) TEM images of $Pt_3Co/C(Li_{0.6})$-700 °C-2 h after ADT. (**d**) Size distribution histogram of $Pt_3Co/C(Li_{0.6})$-700 °C-2 h after ADT.

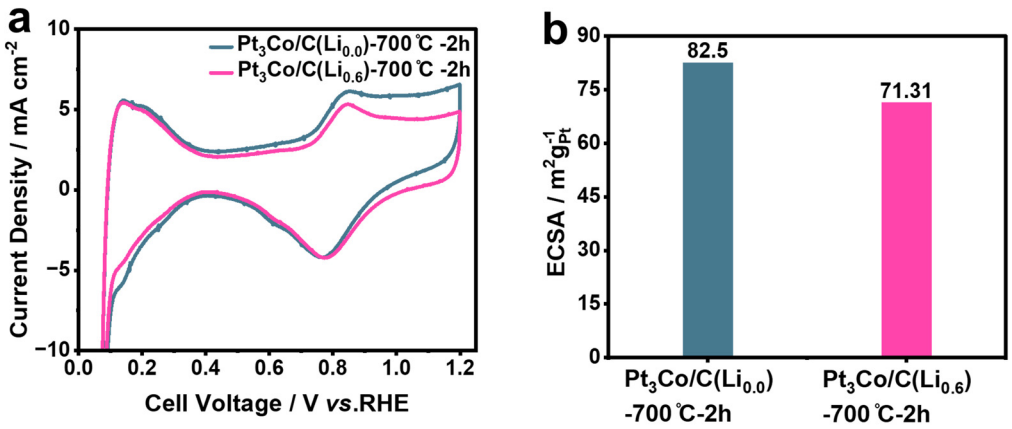

Figure S15. (**a**) Comparison of CV curves for $Pt_3Co/C(Li_{0.0})$-700 ° C-2 h and $Pt_3Co/C(Li_{0.6})$-700 ° C-2 h. (**b**) Comparison of ECSA for $Pt_3Co/C(Li_{0.0})$-700 °C-2 h and $Pt_3Co/C(Li_{0.6})$-700 °C-2 h.

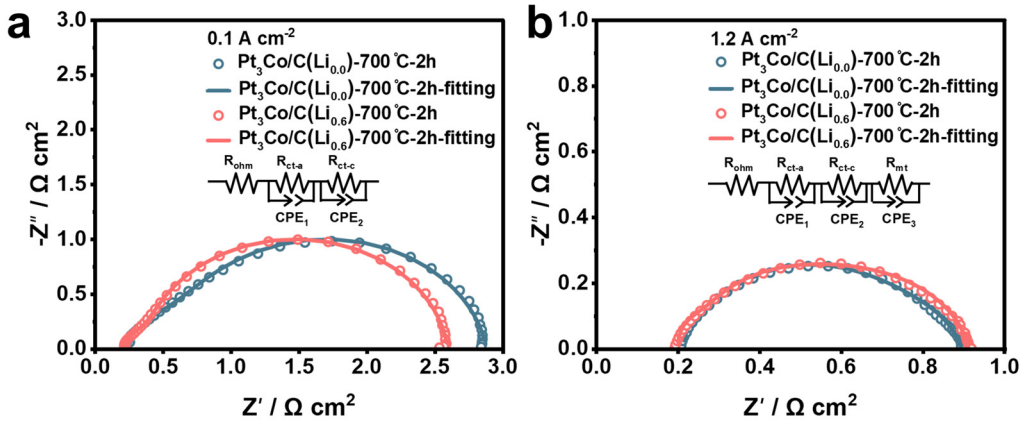

Figure S16. (**a**) Nyquist plots of EIS spectra recorded at 0.1 A cm^{-2} for $Pt_3Co/C(Li_{0.0})$-700 ° C-2 h and $Pt_3Co/C(Li_{0.6})$-700 ° C-2 h. (**b**) Nyquist plots of EIS spectra recorded at 1.2 A cm^{-2} for $Pt_3Co/C(Li_{0.0})$-700 ° C-2 h and $Pt_3Co/C(Li_{0.6})$-700 ° C-2 h.

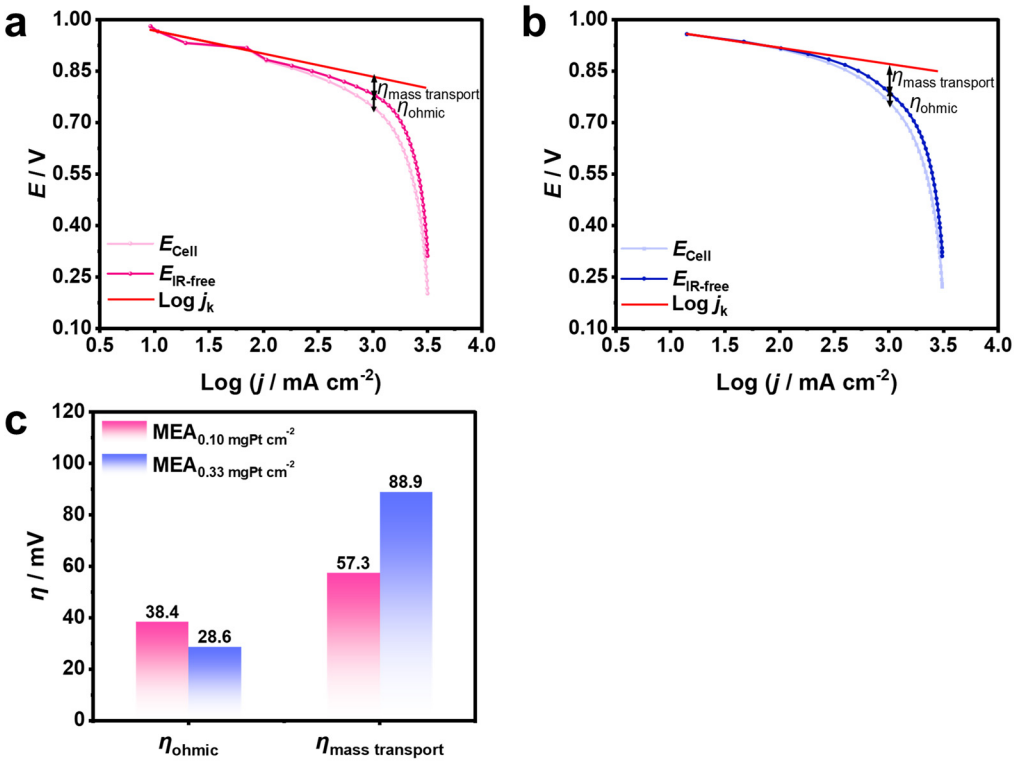

Figure S17. (**a**) Tafel plots and overpotential analysis for $MEA_{0.10\ mgPt\ cm^{-2}}$ under H_2-air. (**b**) Tafel plots and overpotential analysis for $MEA_{0.33\ mgPt\ cm^{-2}}$ under H_2-air. (**c**) Comparison of η_{ohmic} and $\eta_{mass\ transport}$ for $MEA_{0.10\ mgPt\ cm^{-2}}$ and $MEA_{0.33\ mgPt\ cm^{-2}}$.

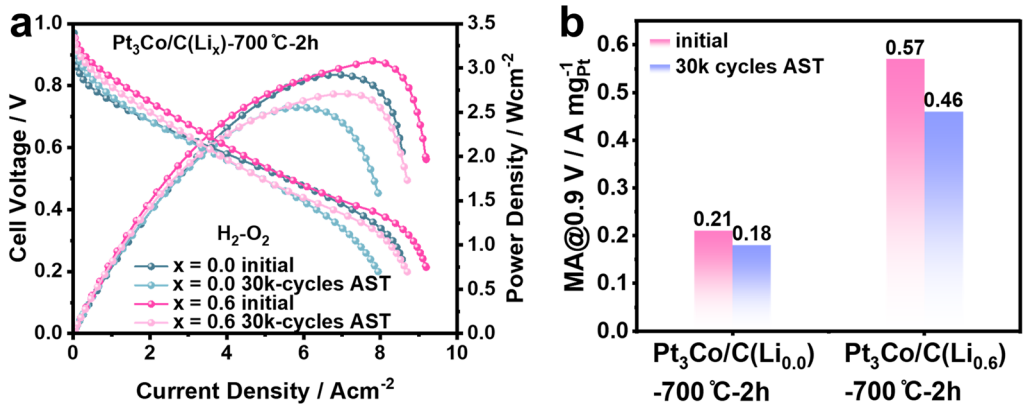

Figure S18. (**a**) Comparison of steady-state polarization curves of the $Pt_3Co/C(Li_{0.0})$-700 °C-2 h and $Pt_3Co/C(Li_{0.6})$-700 °C-2 h before and after AST under H_2-air. (**b**) Comparison of MA for $Pt_3Co/C(Li_{0.0})$-700 °C-2 h and $Pt_3Co/C(Li_{0.6})$-700 °C-2 h before and after AST.

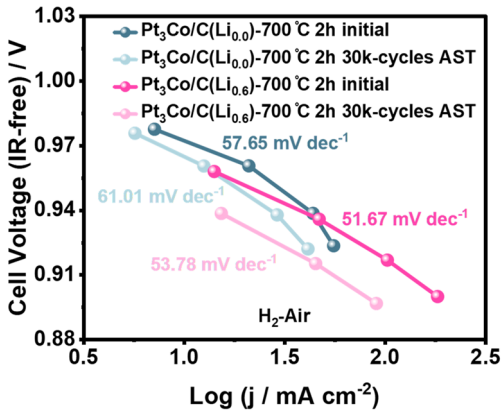

Figure S19. Tafel curves of the $Pt_3Co/C(Li_{0.0})$-700 °C-2 h and $Pt_3Co/C(Li_{0.6})$-700°C-2 h before and after AST under H_2-air.

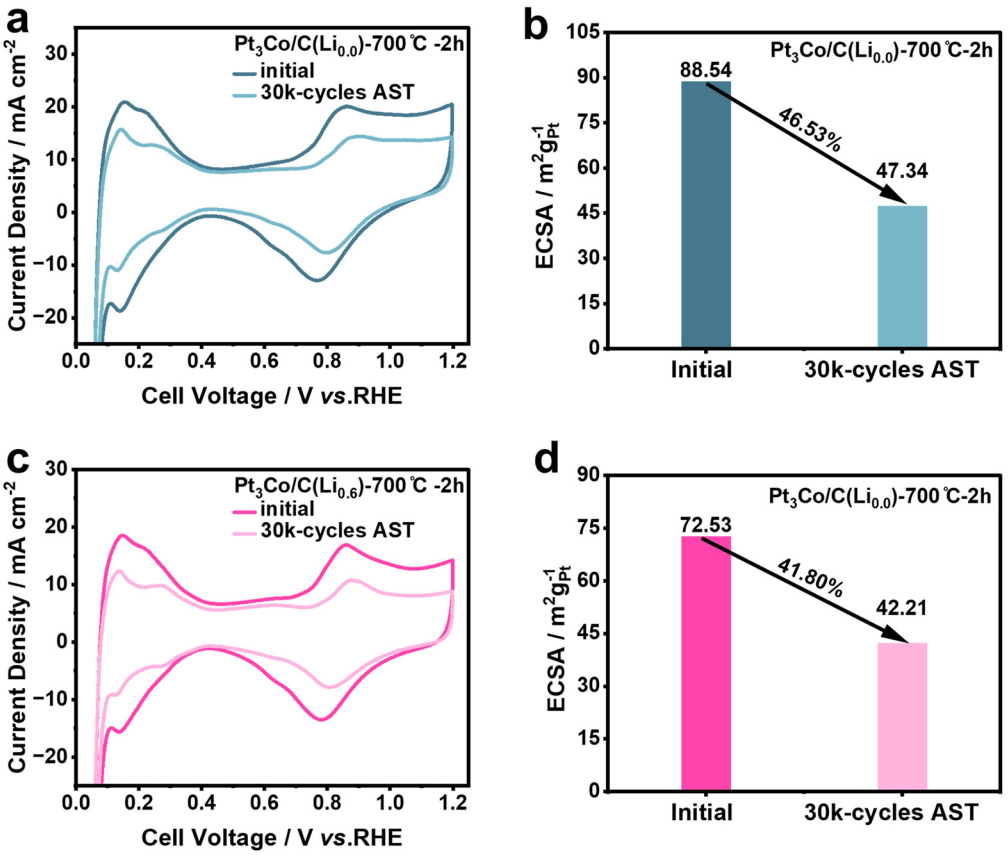

Figure S20. (**a**) Comparison of CV curves for $Pt_3Co/C(Li_{0.0})$-700 ° C-2 h before and after AST. (**b**) Comparison of ECSA for $Pt_3Co/C(Li_{0.0})$-700 °C-2 h before and after AST. (**c**) Comparison of CV curves for $Pt_3Co/C(Li_{0.6})$-700 ° C-2 h before and after AST. (**d**) Comparison of ECSA for $Pt_3Co/C(Li_{0.6})$-700 °C-2 h before and after AST.

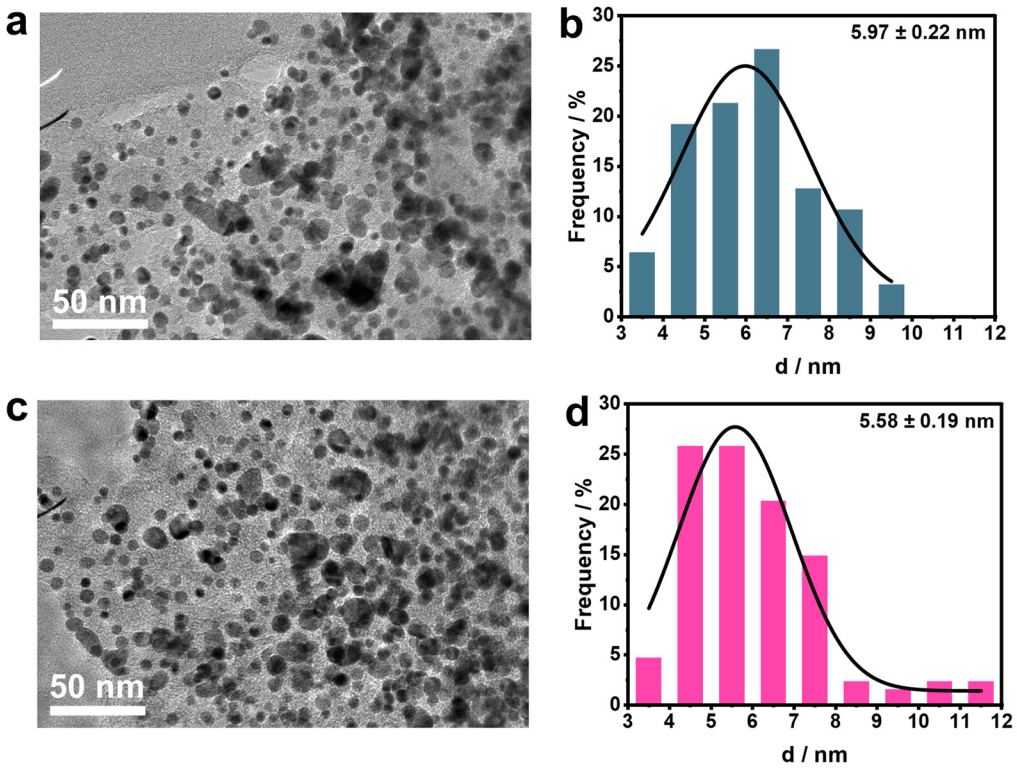

Figure S21. (**a**)TEM images of $Pt_3Co/C(Li_{0.0})$-700 °C-2 h after AST. (**b**) Size distribution histogram of $Pt_3Co/C(Li_{0.0})$-700 °C-2 h after AST. (**c**) TEM images of $Pt_3Co/C(Li_{0.6})$-700 °C-2 h after AST. (**d**) Size distribution histogram of $Pt_3Co/C(Li_{0.6})$-700 °C-2 h after AST.

Table S1. The mass fractions and atomic ratios of each element in different samples (The mass fraction was determined by ICP-OES).

Sample ($Pt_3Co/C(Li_x)$-700 °C-2 h)	Pt /wt.%	Co /wt.%	Li /wt.%	Atomic ratio Pt:Co:Li
***x* = 0.0**	49.12	5.15	0.00	1:0.34
***x* = 0.3**	47.15	4.41	0.20	1:0.31:0.12
***x* = 0.5**	50.36	4.54	0.19	1:0.30:0.11
***x* = 0.6**	50.43	5.46	0.21	1:0.36:0.12
***x* = 0.7**	51.46	5.63	0.22	1:0.36:0.12
***x* = 1.0**	48.91	5.32	0.27	1:0.36:0.15
***x* = 0.6 (after washing)**	52.30	4.57	0.013	1:0.29:0.007

Table S2. Comparison of particle size (*d*) and Pt loading between $Pt_3Co/C(Li_{0.6})$-700 °C-2 h and previously reported conventional PtM-IMC catalysts.

Catalysts	Pt loading (wt%)	*d* (nm)	Refs.
$Pt_3Co/C(Li_{0.6})$-700 °C-2 h	50.43	3.58 ± 0.02	This work
PtCoNiGaZn@Pt/C	40.53	3.15	1
PtCo-O/C-6	30.6	3.2 ± 1.0	2
O-Pt_3Co/NC1100	12.5	4.6	3
$L1_0$-PtPdFe/C	22.8	6.12 ± 0.8	4
i-CoPt@Pt/KB	40.05	< 5	5
PtFe/NcPS	4.8	1.48 ± 0.82	6
Pt_3Co/Te-C	18.2	4.2 ± 1.03	7
Pt_1Co_1-IMC@Pt/C	44.7	5.6	8
DC-Pt_1Co_1/CNT	8	≈ 4	9
$L1_0$-NPtCo@Pt/C	21.8	≈ 5	10

Table S3. Analysis of Pt 4*f* XPS peak including peak position, half peak width and integral area.

Sample	Pt^0(eV)		Pt^{2+}(eV)		Pt^0	Pt^{2+}
($Pt_3Co/C(Li_x)$-700 °C-2 h)	$4f_{7/2}$	$4f_{5/2}$	$4f_{7/2}$	$4f_{5/2}$	4*f* (%)	4*f* (%)
***x* = 0.0**	71.75	75.10	72.87	76.37	52.49	47.51
***x* = 0.3**	71.85	75.19	73.08	76.55	53.14	46.86
***x* = 0.5**	71.82	75.16	73.03	76.53	54.08	45.92
***x* = 0.6**	71.80	75.16	73.03	76.53	55.24	44.76
***x* = 0.7**	71.83	75.17	72.93	76.43	52.60	47.40
***x* = 1.0**	71.81	75.15	72.94	76.43	52.60	47.40

All XPS spectra were fitted using Gaussian-Lorentzian peak shapes. The binding energy scale was calibrated using adventitious carbon (C 1*s* at 284.80 eV). For Pt 4*f* spectra, the doublet separation was fixed at 3.35 eV with an area ratio of 4:3 (Pt $4f_{7/2}$ Pt $4f_{5/2}$).

Table S4. The fitting parameters of Pt L_3-edge for various samples.

Sample	Path	*CN*	*R*(Å)	σ^2(Å^2)	ΔE_0 (eV)	*R* factor
Pt foil	Pt-Pt	12.11	2.76	0.0046	5.46	0.0183
PtO_2	Pt-O	5.48	2.02	0.0025	0.0599	0.0187
	Pt-O	1.15	1.99	0.0026		
$Pt_3Co/C(Li_{0.0})$-600℃	Pt-Co	0.88	2.66	0.0095	0.8590	0.0142
	Pt-Pt	7.09	2.72	0.0095		
	Pt-O	0.31	1.98	0.0000		
$Pt_3Co/C(Li_{0.0})$-700℃-2h	Pt-Co	1.27	2.68	0.0080	0.8853	0.0133
	Pt-Pt	9.12	2.71	0.0080		
	Pt-O	0.33	1.98	0.0000		
$Pt_3Co/C(Li_{0.6})$-300℃	Pt-Cl	0.57	2.26	0.0087	0.3014	0.0040
	Pt-Pt	8.05	2.74	0.0087		
	Pt-O	0.67	1.99	0.0024		
$Pt_3Co/C(Li_{0.6})$-600℃	Pt-Co	0.92	2.67	0.0090	0.2511	0.0092
	Pt-Pt	8.69	2.72	0.0090		
	Pt-O	0.25	1.99	0.0000		
$Pt_3Co/C(Li_{0.6})$-700℃-2h	Pt-Co	1.56	2.68	0.0076	0.5270	0.0089
	Pt-Pt	9.13	2.72	0.0076		

CN, coordination numbers; *R*, distance between absorber and backscatter atoms; σ^2, Debye-Waller factor to account for both thermal and structural disorders; $\triangle E_0$, inner potential correction; *R*-factor, a measure of the quality of the EXAFS fit.

Table S5. Particle size distribution and diffraction peak position (DPP) changes of (111), (200), and (220) planes at different temperatures for $Pt_3Co/C(Li_{0.0})$ and $Pt_3Co/C(Li_{0.6})$.

T	$DPP_{(111)}$		$DPP_{(200)}$		$DPP_{(220)}$	
	$Pt_3Co/C(Li_{0.0})$	**$Pt_3Co/C(Li_{0.6})$**	**$Pt_3Co/C(Li_{0.0})$**	**$Pt_3Co/C(Li_{0.6})$**	**$Pt_3Co/C(Li_{0.0})$**	**$Pt_3Co/C(Li_{0.6})$**
200 °C	/	39.73	/	46.25	/	67.53
300 °C	39.78	39.90	46.27	46.44	67.67	68.40
400 °C	40.28	40.39	46.54	46.61	68.24	68.45
500 °C	40.38	40.51	46.78	47.10	68.49	68.78
600 °C	40.52	40.53	47.23	47.18	68.69	68.79
700 °C	40.53	40.57	47.22	47.20	68.95	69.03
700 °C-2 h	40.82	40.58	47.35	47.22	69.07	69.04

Table S6. MA, SA, ECSA, and $E_{1/2}$ of $Pt_3Co/C(Li_x)$-700 °C-2 h.

Sample ($Pt_3Co/C(Li_x)$-700 °C-2 h)	**MA@0.9 V** A mg_{Pt}^{-1}	**SA@0.9 V** mA cm^{-2}	**ECSA** m^2 g_{Pt}^{-1}	$E_{1/2}$ V *vs.* RHE
***x* = 0.0**	0.55 ± 0.01	1.03 ± 0.01	52.62 ± 0.39	0.922 ± 0.004
***x* = 0.3**	0.60 ± 0.05	1.19 ± 0.07	52.13 ± 0.24	0.929 ± 0.004
***x* = 0.5**	0.66 ± 0.02	1.31 ± 0.01	50.32 ± 0.81	0.926 ± 0.002
***x* = 0.6**	0.86 ± 0.04	1.75 ± 0.07	49.23 ± 0.61	0.934 ± 0.004
***x* = 0.7**	0.62 ± 0.00	1.28 ± 0.01	48.97 ± 0.28	0.928 ± 0.001
***x* = 1.0**	0.60 ± 0.04	1.23 ± 0.06	48.41 ± 0.49	0.920 ± 0.002

Table S7. EIS parameters of the MEA at 0.1 and 1.2 A cm^{-2}.

Catalyst	0.1 A cm^{-2}		1.2 A cm^{-2}		
	R_{ohm} / Ω cm^2	$R_{ct\text{-}c}$ / Ω cm^2	R_{ohm} / Ω cm^2	$R_{ct\text{-}c}$ / Ω cm^2	R_{mt} / Ω cm^2
$Pt_3Co/C(Li_{0.0})$-700℃-2h	0.23	2.27	0.22	0.39	0.23
$Pt_3Co/C(Li_{0.6})$-700℃-2h	0.22	2.23	0.20	0.25	0.42

Table S8. Comparison of ORR activity and durability between $Pt_3Co/C(Li_{0.6})$-700℃-2h and previously reported conventional PtM-IMC catalysts.

Catalysts	MA @0.9V(RDE) A mg_{Pt}^{-1}	PPD / Wcm^{-2}		MA Loss (AST) %	Refs.
		H_2-Air	H_2-O_2		
$Pt_3Co/C(Li_{0.6})$-700℃-2h	0.86	1.23	2.92	19.3	This work
PtCoNiGaZn@Pt/C	0.65	0.96	2.44	12.5	1
PtCo-O/C-6	1.28	1.25	2.38	18.5	2
O-Pt_3Co/NC1100	1.21	1.27	-	-	3
$L1_0$-PtPdFe/C	0.89	-	-	32.8	4
i-CoPt@Pt/KB	2.07	1.18	-	35.5	5
PtFe/NcPS	1.35	-	-	33.8	6
Pt_3Co/Te-C	0.30	-	2.32	26	7
Pt1Co1-IMC@Pt/C	0.53	1.23	2.30	24.8	8
Pt_3Ga	2.18	1.06	-	-	11
$Pt_{56}Mn_{44}$	0.53	-	1.36	-	12
PtNiMoAu NWs/C	2.42	0.92	1.75	22.6	13
PtCo@Gnp	-	1.01	-	34.2	14
$L1_0$-CoPt/Pt	-	1.1	-	19.6	15
$L1_0$-Cr-PtFe/C	2.05	1.15	-	25	16

Reference

1 Y. Pan, Y. Chen, Y. Li, M. Liu, L. Yao, H. Zhao, X. Zhao, Z. Yue, S. Gui, Y. Chen, Q. Cheng and H. Yang, *Adv. Funct. Mater.*, 2025, 2503628.

2 F. Kong, Y. Huang, X. Yu, M. Li, K. Song, Q. Guo, X. Cui and J. Shi, *J. Am. Chem. Soc.*, 2024, **146**, 30078–30090.

3 W. Xu, Z. Zhu, Y. Wang, P. Cui, L. Tong, K. Zhao, J. Yuan, Z.-Y. Zhou, H.-W. Liang, N. Tian and S.-G. Sun, *J. Mater. Chem. A.*, 2023, **11**, 4078–4087.

4 M. I. Maulana, J. Kim, H.-Y. Lee, C. Gyan-Barimah, Y. Wei, J.-H. Yu, J. H. Sung, B. Yu, K.-S. Lee, S. Back and J.-S. Yu, *Adv. Mater.*, 2025, e10314.

5 T. Y. Yoo, J. Lee, S. Kim, M. Her, S.-Y. Kim, Y.-H. Lee, H. Shin, H. Jeong, A. K. Sinha, S.-P. Cho, Y.-E. Sung and T. Hyeon, *Energy Environ. Sci.*, 2023, **16**, 1146–1154.

6 S. Shin, E. Lee, J. Nam, J. Kwon, Y. Choi, B. J. Kim, H. C. Ham and H. Lee, *Adv. Energy Mater.*, 2024, **14**, 2400599.

7 Y. Chen, Z. Meng, F. Liu, A. Zhang, X. Wang, Y. Xiong, H. Tang, T. Tian and H. Tang, *Adv. Funct. Mater.*, 2024, **34**, 2408383.

8 Q. Cheng, S. Yang, C. Fu, L. Zou, Z. Zou, Z. Jiang, J. Zhang and H. Yang, *Energy Environ. Sci.*, 2022, **15**, 278–286.

9 L. Tian, X. Gao, M. Zhu, Z. Huang, B. Wu, C. Chen, X. Ma, Y. Ruan, W. Guo, X. Meng, H. Wang, W. Du, S. He, H. Pan, X. Zheng, Z. Wu, H. Zhou, J. Xia and Y. Wu, *Adv. Mater.*, 2025, **37**, 2417095.

10 M. I. Maulana, T. H. Jo, H.-Y. Lee, C. Lee, C. Gyan-Barimah, C.-H. Shin, J.-H. Yu, K.-S. Lee, S. Back and J.-S. Yu, *J. Am. Chem. Soc.*, 2024, **146**, 30922-30932.

11 R. Gui, H. Cheng, M. Wang, X. Tai, H. Zhang, C. Liu, X. Cao, C. Chen, M. Ge, H. Wang, X. Zheng, W. Chu, Y. Lin, Y. Xie and C. Wu, *Adv. Mater.*, 2024, **36**, 2307661.

12 Y. Nie, Y. Sun, B. Song, Q. Meyer, S. Liu, H. Guo, L. Tao, F. Lin, M. Luo, Q. Zhang, L. Gu, L. Yang, C. Zhao and S. Guo, *Angew. Chem.*, 2024, **136**, e202317987.

13 L. Gao, T. Sun, X. Chen, Z. Yang, M. Li, W. Lai, W. Zhang, Q. Yuan and H. Huang, *Nat. Commun.*, 2024, **15**, 508.

14 Z. Zhao, Z. Liu, A. Zhang, X. Yan, W. Xue, B. Peng, H. L. Xin, X. Pan, X. Duan and Y. Huang, *Nat. Nanotechnol.*, 2022, **17**, 968–975.

15 Y.-T. Pan, D. Li, S. Sharma, C. Wang, M. J. Zachman, E. C. Wegener, A. J. Kropf, Y. S. Kim, D. J. Myers, A. A. Peterson, D. A. Cullen and J. S. Spendelow, *Chem Catal.*, 2022, **2**, 3559–3572.

16 X. Liu, Y. Wang, J. Liang, S. Li, S. Zhang, D. Su, Z. Cai, Y. Huang, L. Elbaz and Q. Li, *J. Am. Chem. Soc.*, 2024, **146**, 2033–2042.